Computers & Structures Vol. 49, No. 3, pp. 399–410, 1993
Printed in Great Britain.

0045-7949/93 $6.00 + 0.00

FINITE ELEMENT VIBRATION ANALYSIS OF A HELICALLY WOUND TUBULAR AND LAMINATED COMPOSITE MATERIAL BEAM

C. I. CHEN, V. H. MUCINO and E. J. BARBERO
Department of Mechanical and Aerospace Engineering, West Virginia University, Morgantown, WV 26505, U.S.A.

(*Received* 14 *July* 1992)

Abstract—Finite element stiffness and consistent mass matrices are derived for helically wound, symmetrical composite tubes. The tubular element is considered to have constant cross-section and small deformations restricted to a plane. Each node has three degrees of freedom: axial and transverse displacement and rotation (slope of transverse displacement). Shell theory and lamination theory are used to formulate element stiffness matrices. The stiffness and mass matrices derived from the helically wound tubular composite material are reduced to symmetrically laminated composite beam. The free vibration and natural frequency are investigated for five different materials: steel, aluminum, carbon/N5280, Kevlar-49/epoxy and graphite/epoxy composites and various layup configurations. One application of a rotating flexible beam is investigated. The dynamic model of the flexible rotating beam includes the coupled effect between the rigid body motion and the flexible motion. The inverse dynamic simulation is performed by a prescribed driving torque in the numerical simulation. The influence of flexibility on rigid body motion are presented and discussed. From the numerical results, the composite material strongly possesses the lower power consumption and the passive control in damping the vibration of the structure.

INTRODUCTION

The dynamic modeling of structures with beam or rod elements has been well developed in the past, especially the area of dynamic analysis of multibody mechanism systems, such as four-bar mechanism, crank–slider mechanism and robotic manipulator. The rigid body assumption in the analysis of multibody systems is not adequate due to high operation speeds, large external load and high precision requirements. The analysis of flexible links in the multibody systems has been developed in the past two decades [1–5]. Generally speaking, research in this area can be divided into two categories: The first treats the elastic links of the mechanical system as a continuous system [6–10]. The equations of motion for these continuous systems are derived with the help of certain simplifying assumptions and solved to obtain the system response. In the second category, the elastic links of the system are modeled as discrete systems via finite element formulations [11–15]. The advantages of the finite element formulations are that they provide an easier and systematic modeling technique for complex mechanical systems. The drawback of the second method is the requirement of substantial computer time simulation due to the many degrees of freedoms in the system. However, modal synthesis can be utilized to reduce the degrees of freedom. In addition, the accuracy of the dynamic response depends on the selection of the modal degrees of freedoms [16, 17]. Furthermore, most of the work in this area considered flexible bodies made of isotropic materials. Recently, an alternative philosophy has been proposed for the design of flexible multibody systems which requires the members to be fabricated with advanced composite materials [18–24]. Generally speaking, composite materials possess much higher strength-to-weight ratios and stiffness-to-weight ratios than metals. Consequently, the systems experience much smaller deflections when subject to load.

Thompson [18, 19] used an elastic continuous model for a fibrous composite material to predict the global features of the dynamic response of a four-bar mechanism fabricated from a graphite/epoxy material. The results of the study demonstrate how vibrational activity in high-speed machinery can be reduced by fabricating members from a composite laminate rather than commercial metals. Shabana [22] presented a finite element scheme for studying the dynamic response of crank–slider and Peucellier mechanism with components manufactured from orthotropic material. They concluded that composite materials can be treated as an effective passive control system. D'Acquisto [23] developed a finite element model for the preliminary design of a helically wound tubular composite structure which can be used as links of high-speed mechanisms. Krishnamurthy *et al.* [24] investigated a dynamic model for single-link robotic arms from orthotropic composite materials. Chen and Yang [25] presented a finite element model for anisotropic symmetrically

laminated beam including the effect of shear deformation and torsional deformation.

The main objective of this study is to formulate the mass and the stiffness matrices of laminate tubular beam element to conduct the dynamic analysis of composite laminate beam structure with future application to the flexible multibody systems. The mass and stiffness matrices of a tubular beam derived in this paper are also reduced to fiber-reinforced orthotropic material with a symmetrically laminated composite rectangular cross-section. Validation of the element with the existing analytical solution for a rectangular cross-section is presented. The free vibration of natural frequency is analyzed in terms of five materials: steel, aluminum, carbon/N5280 composite, Kevlar-49/epoxy and graphite/epoxy composite. Various layups of each composite material are considered. A flexible rotating beam is considered as one application based on the matrices developed in this study. The coupled effect between the rigid body motion and the flexible motion is included. The inverse dynamic simulation is performed by a prescribed driving torque in the numerical simulation. The influence of flexibility on rigid body motion is presented and discussed. It can be shown that the composite material strongly possesses the passive control in damping the vibration of the structure.

LAMINATE SHELL THEORY

In a laminated on composite material, a lamina is a single layer with thickness h, with a unidirectional or woven fiber orientation at angle θ from a local coordinate axis as shown in Fig. 1. A laminate is a stack of laminae with various orientations of principal material directions in the laminae. In combining shell theory with lamination theory, the assumption is made that each composite lamina can be analyzed as a thin cylindrical shell and elastic deformations are assumed to be small within the linear range. The relation of stress and strain for a particular layer k in local coordinate can be expressed as

$$\begin{Bmatrix}\sigma_x\\ \sigma_\phi\\ \tau_{x\phi}\end{Bmatrix}^{(k)} = \begin{bmatrix}\bar{Q}_{11} & \bar{Q}_{12} & \bar{Q}_{16}\\ \bar{Q}_{21} & \bar{Q}_{22} & \bar{Q}_{26}\\ \bar{Q}_{16} & \bar{Q}_{26} & \bar{Q}_{66}\end{bmatrix}^{(k)} \begin{Bmatrix}\epsilon_x\\ \epsilon_\phi\\ \gamma_{x\phi}\end{Bmatrix}^{(k)}, \quad (1)$$

where ϕ is the polar coordinate. $[\bar{Q}]^{(k)}$ is the transformed reduced stiffness matrix and is given by

$$\begin{aligned}
\bar{Q}_{11} &= Q_{11}\cos^4\theta + 2(Q_{12} + 2Q_{66})\sin^2\theta\cos^2\theta + Q_{22}\sin^4\theta\\
\bar{Q}_{12} &= (Q_{11} + Q_{22} - 4Q_{66})\sin^2\theta\cos^2\theta + Q_{12}(\sin^4\theta + \cos^4\theta)\\
\bar{Q}_{22} &= Q_{11}\sin^4\theta + 2(Q_{12} + 2Q_{66})\sin^2\theta\cos^2\theta + Q_{22}\cos^4\theta\\
\bar{Q}_{16} &= (Q_{11} - Q_{12} - 2Q_{66})\sin\theta\cos^3\theta + (Q_{12} - Q_{22} + 2Q_{66})\sin^3\theta\cos\theta\\
\bar{Q}_{26} &= (Q_{11} - Q_{12} - 2Q_{66})\sin^3\theta\cos\theta + (Q_{12} - Q_{22} + 2Q_{66})\sin\theta\cos^2\theta\\
\bar{Q}_{66} &= (Q_{11} + Q_{22} - 2Q_{12} - 2Q_{66})\sin^2\theta\cos^2\theta + Q_{66}(\sin^4\theta + \cos^4\theta)
\end{aligned} \quad (2)$$

where θ is the angle from the x-axis to the 1-axis and Q_{ij} are the so-called reduced stiffnesses and can be expressed in terms of engineering constants [26] where $\gamma_{x\phi} = 2\epsilon_{x\phi}$. Neglecting the high order terms, the

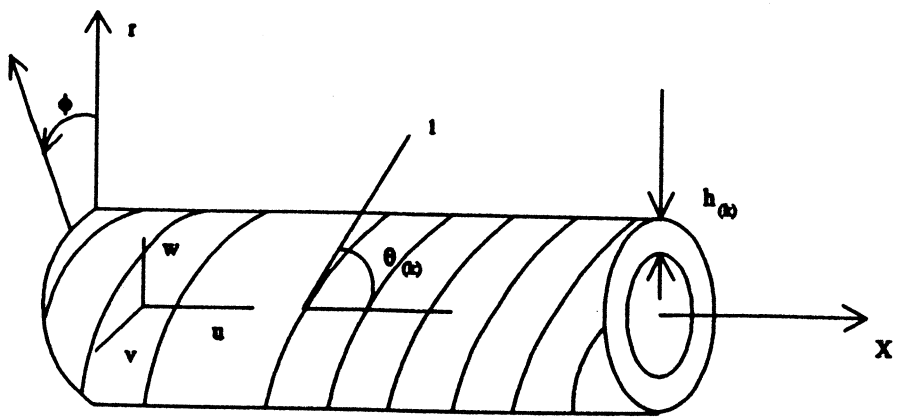

Fig. 1. Schematic of the kth ply in the tubular element.

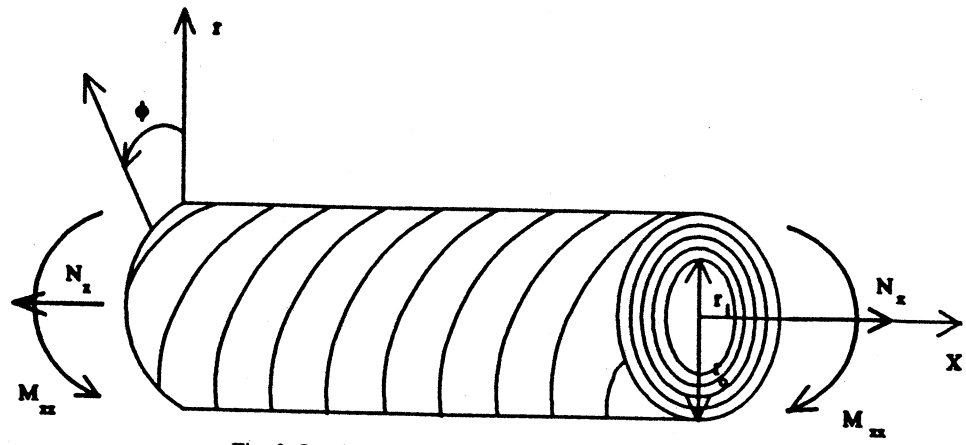

Fig. 2. Laminated helically wound beam configuration.

kinematic equations of a cylindrical element can be expressed by [27]

$$\begin{Bmatrix} \epsilon_x \\ \epsilon_\phi \\ \epsilon_{x\phi} \end{Bmatrix} = \begin{Bmatrix} \epsilon_x^0 + zX_x \\ \epsilon_\phi^0 + z\left(1 - \frac{z}{a}\right)X_\phi \\ \left[1 + \frac{z^2}{2a^2}\right]\epsilon_{x\phi}^0 + 2z\left[1 - \frac{z}{2a}\right]X_{x\phi} \end{Bmatrix}, \quad (3)$$

where the membrane strains in the reference surface of the shell are

$$\begin{Bmatrix} \epsilon_x^0 \\ \epsilon_\phi^0 \\ \epsilon_{x\phi}^0 \end{Bmatrix} = \begin{Bmatrix} \frac{\partial u}{\partial x} \\ \frac{1}{a}\left(\frac{\partial v}{\partial \phi} + w\right) \\ \frac{1}{a}\frac{\partial u}{\partial \phi} + \frac{\partial v}{\partial x} \end{Bmatrix} \quad (4)$$

and the changes in curvature and twist of the reference surface are

$$X_x = -\frac{\partial^2 w}{\partial x^2}$$

$$X_\phi = -\frac{1}{a^2}\left(\frac{\partial v}{\partial \phi} + w\right)$$

$$X_{x\phi} = -\frac{1}{a}\left(\frac{\partial^2 w}{\partial x \partial \phi} + \frac{1}{2a}\frac{\partial u}{\partial \phi} - \frac{1}{2}\frac{\partial v}{\partial x}\right). \quad (5)$$

where a is the average radius of the cylinder; u, v, and w are the deformations associated with x, ϕ and r axes, respectively. The resultant force N and moment M are obtained by integration of the stresses in each lamina through the laminae thickness as shown in Fig. 2. For example

$$N_x = \int_{-h/2}^{h/2} \sigma_x\left(1 + \frac{z}{a}\right)dz \quad (6)$$

$$M_x = \int_{-h/2}^{h/2} \sigma_x\left(1 + \frac{z}{a}\right)z\, dz. \quad (7)$$

Substituting eqn (1) into (6) and (7) and integrating through the laminae thickness, the final result can be written in a compact form as

$$\begin{Bmatrix} N_x \\ N_\phi \\ N_{x\phi} \\ N_{\phi x} \\ M_x \\ M_\phi \\ M_{x\phi} \\ M_{\phi x} \end{Bmatrix} = \begin{bmatrix} A_{11} + \frac{B_{11}}{a} & A_{12} + \frac{B_{12}}{a} & A_{16} + \frac{B_{16}}{a} + \frac{D_{16}}{2a^2} & B_{11} + \frac{D_{11}}{a} & B_{12} & B_{16} + \frac{D_{16}}{2a} \\ A_{12} & A_{22} & A_{26} + \frac{D_{26}}{2a^2} & B_{12} & B_{22} - \frac{D_{22}}{a} & B_{26} - \frac{D_{26}}{2a} \\ A_{16} + \frac{B_{16}}{a} & A_{26} + \frac{B_{26}}{a} & A_{66} + \frac{B_{66}}{a} + \frac{D_{66}}{2a^2} & B_{16} + \frac{D_{16}}{a} & B_{26} & B_{66} + \frac{D_{66}}{2a} \\ A_{16} & A_{26} & A_{66} + \frac{D_{66}}{2a^2} & B_{16} & B_{26} - \frac{D_{26}}{a} & B_{66} - \frac{D_{66}}{2a} \\ B_{11} + \frac{D_{11}}{a} & B_{12} + \frac{D_{16}}{a} & B_{16} + \frac{D_{16}}{a} & D_{11} & D_{12} & D_{16} \\ B_{12} & B_{22} & B_{26} & D_{12} & D_{22} & D_{26} \\ B_{16} + \frac{D_{16}}{a} & B_{26} + \frac{D_{26}}{a} & B_{66} + \frac{D_{66}}{a} & D_{16} & D_{26} & D_{66} \\ B_{16} & B_{26} & B_{66} & D_{16} & D_{26} & D_{66} \end{bmatrix} \begin{Bmatrix} \epsilon_x^0 \\ \epsilon_\phi^0 \\ \epsilon_{x\phi}^0 \\ X_x \\ X_\phi \\ X_{x\phi} \end{Bmatrix}, \quad (8)$$

where

$$A_{ij} = \sum_{k=1}^{N} \bar{Q}_{ij}^{(k)}(h_{(k)} - h_{(k-1)})$$

$$B_{ij} = \sum_{k=1}^{N} \frac{1}{2}\bar{Q}_{ij}^{(k)}(h_{(k)}^2 - h_{(k-1)}^2)$$

$$D_{ij} = \sum_{k=1}^{N} \frac{1}{3}\bar{Q}_{ij}^{(k)}(h_{(k)}^3 - h_{(k-1)}^3). \quad (9)$$

For the classical lamination beam theory, we assumed that the laminate consists of perfectly bonded laminae, bonds are infinitesimally thin, and shear deformation is negligible. The displacements are continuous across lamina boundaries so that no lamina can slip relative to another. Furthermore, only small deformations are considered in the context of thin plate theory. A line originally straight and perpendicular to the middle surface of the laminate is assumed to remain straight and normal when the laminate is extended and bent. Due to the assumption of axisymmetry with respect to the neutral axis of the beam and neglecting Poisson effects, eqn (8) can be simplified to [23]

$$\begin{Bmatrix} N_x \\ M_x \end{Bmatrix} = \begin{bmatrix} A_{11} + \dfrac{B_{11}}{a} & B_{11} + \dfrac{D_{11}}{a} \\ B_{11} + \dfrac{D_{11}}{a} & D_{11} \end{bmatrix} \begin{Bmatrix} \epsilon_x^0 \\ K_x \end{Bmatrix}, \quad (10)$$

where $\epsilon_x^0 = \partial u/\partial x$, $K_x = -\partial^2 w/\partial x^2$ and u and w are the axial transverse deformations, respectively. For a rectangular beam, a approaches infinity and eqn (10) reduces to the well known expression for laminated beams if all Poisson ratios are taken to be zero [29].

EQUATION OF MOTION

The equations of motion for a typical element are derived using the Lagrangian function. A typical element configuration and coordinate system are shown in Fig. 3, with l the length of the element, and ξ the nondimensional parameter defined by $\xi = x/l$. The generalized coordinates e_1, e_2, e_3, e_4, e_5 and e_6 represent elastic deformations at the nodal points. The deformation at an arbitrary point in the element is approximated in terms of e_1, e_2, e_3, e_4, e_5, and e_6 and the shape functions as

$$\begin{Bmatrix} u(\xi, t) \\ w(\xi, t) \end{Bmatrix} = \begin{bmatrix} N_1 & 0 & 0 & N_2 & 0 & 0 \\ 0 & N_3 & N_4 & 0 & N_5 & N_6 \end{bmatrix} \begin{Bmatrix} e_1 \\ e_2 \\ e_3 \\ e_4 \\ e_5 \\ e_6 \end{Bmatrix}, \quad (11)$$

where N_i are the shape functions and are given by

$$N_1 = 1 - \xi$$

$$N_2 = \xi$$

$$N_3 = 1 - 3\xi^2 + 2\xi^3$$

$$N_4 = l(\xi - 2\xi^2 + \xi^3)$$

$$N_5 = 3\xi^2 - 2\xi^3$$

$$N_6 = l(-\xi^2 + \xi^3). \quad (12)$$

The kinetic energy of the beam element is given by

$$T = \tfrac{1}{2}\rho_m A l \int_0^1 (\dot{u} + \dot{w})^2 \, d\xi, \quad (13)$$

where ρ_m, A, and l are the density, the cross-sectional area, and the length of the beam, respectively.

The potential energy stored in the laminated beam is given by

$$V = \tfrac{1}{2} 2\pi a l \int_0^1 [N_x \epsilon_x^0 + M_x k_x] d\epsilon. \quad (14)$$

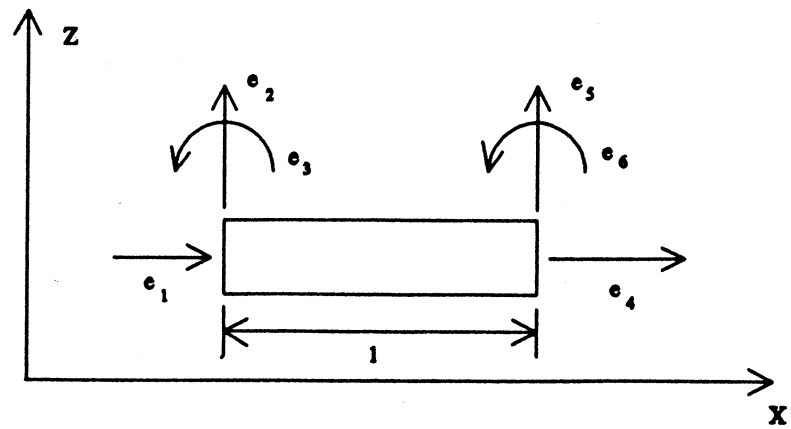

Fig. 3. Generalized coordinates of the beam element.

Table 1. Material properties

	Steel	Aluminum	Carbon/ N5280	Kevlar-49/ epoxy	Graphite/ epoxy
E_1 (Msi)	30.0	10.6	26.25	11.02	20.0
E_2 (Msi)	30.0	10.6	1.49	0.798	1.40
G_{12} (Msi)	11.81	3.98	1.04	0.334	0.8
μ_{12}	0.27	0.33	0.28	0.34	0.3
h (in)	0.25	0.25	0.005	0.005	0.005
E/ρ (10^7 in)	10.6	10.6	45.25	20.8	33.33
ρ_m (lb m/in^3)	0.283	0.1	0.058	0.053	0.06

Substituting eqn (10) into (14) yields

$$V = \pi a l \int_0^1 \left(A_{11} + \frac{D_{11}}{a}\right)\left(\frac{\partial u}{\partial x}\right)^2 - 2\left(B_{11} + \frac{D_{11}}{a}\right)\frac{\partial u}{\partial x}\frac{\partial^2 w}{\partial x^2} + D_{11}\left(\frac{\partial^2 w}{\partial x^2}\right)^2 \mathrm{d}\xi. \quad (15)$$

The equations of motion of the element can be obtained by Lagrange formulation as follows:

$$\frac{\mathrm{d}}{\mathrm{d}t}\frac{\partial L}{\partial \dot{q}_i} - \frac{\partial L}{\partial q_i} = 0, \quad (16)$$

where $L = T - V$ is the Lagrangian. Substituting eqns (13) and (15) into (16), the element equation of motion can be obtained as

$$[M]\{\ddot{q}\} + [K]\{q\} = 0. \quad (17)$$

In eqn (17), $[M]$ and $[K]$ are the mass and the stiffness matrices, respectively, and they are given in the Appendix. The stiffness matrix in eqn (17) can be reduced to the case of a rectangular cross-sectional beam element by assuming a approaches infinity and $2\pi a$ is replaced by the width of the beam. In this case, they coincide with the expressions presented by Cleghorn and Chao [13]. The overall equation of motion is assembled on each element basis with adequate boundary conditions which yields

$$[M_G]\{\ddot{q}_G\} + [K_G]\{q_G\} = \{0\}, \quad (18)$$

where $[M_G]$ and $[K_G]$ are the global mass and stiffness matrices, respectively, and $\{q_G\}$ is the global generalized coordinates. The free vibration of the system with harmonic frequency ω, eqn (18) becomes

$$\{[K_G] - \omega^2[M_G]\}\{q_G\} = \{0\}. \quad (19)$$

Table 2. Geometry parameters

	Rectangular	Tubular
Length (in)	48.00	48.00
Width (in)	0.75	
Thickness (in)	0.25	0.25
Outer diameter (in)		0.75
Inner diameter (in)		0.25

NUMERICAL RESULTS

Both rectangular and tubular cross-sections are considered in this section. The material properties and the geometry parameters are listed in Tables 1 and 2, respectively. Two types of laminates are considered, $a[\pm\alpha]$ angle ply and repeated clusters of $[\alpha/0/-\alpha]_N$, where N is the number of clusters and is taken to be 17 in the numerical results presented. All numerical results illustrate the first five modes. Natural frequencies for all material and both cross-sectional shape (rectangular and tubular) in different layups are shown in Figs 4–17. It can be concluded that the natural frequency depends on the layup and the stiffness-to-weight ratio. The natural frequency of the composite material in a certain fiber angle layup

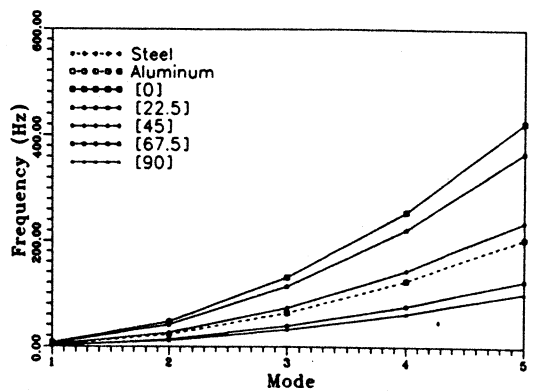

Fig. 4. Frequency variation of fiber angle for carbon/N5280 composite material, with a rectangular cross-section.

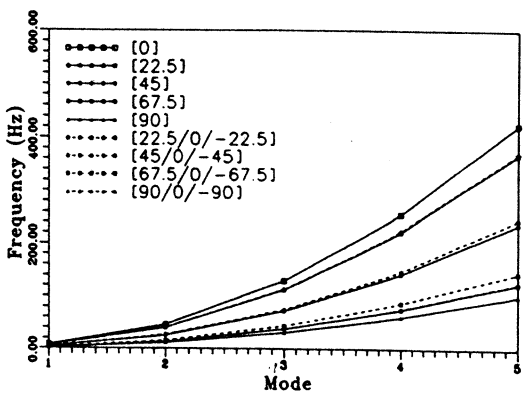

Fig. 5. Frequency of carbon/N5208 composite material, in a different layup, with a rectangular cross-section.

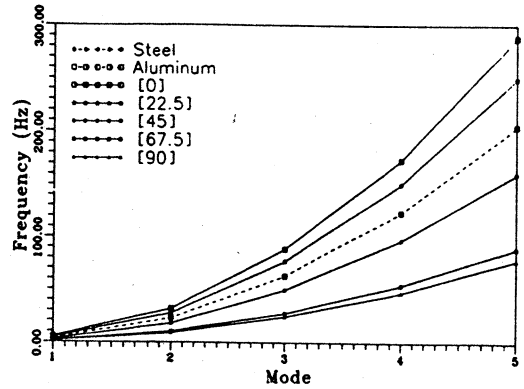

Fig. 6. Frequency variation of fiber angle for Kevlar-49/epoxy composite material, with a rectangular cross-section.

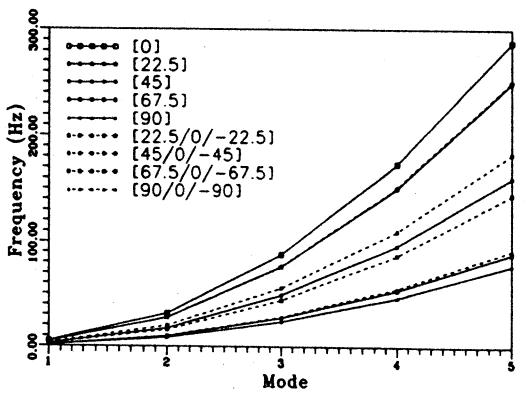

Fig. 7. Frequency of Kevlar-49/epoxy composite material, in a different layup, with a rectangular cross-section.

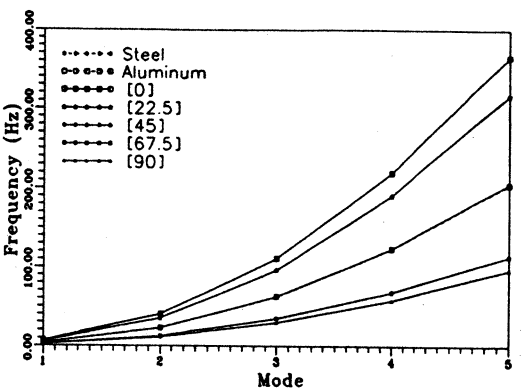

Fig. 8. Frequency variation of fiber angle for graphite/epoxy composite material, with a rectangular cross-section.

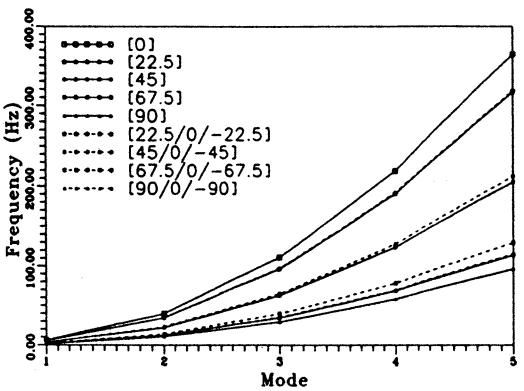

Fig. 9. Frequency of graphite/epoxy composite material, in a different layup, with a rectangular cross-section.

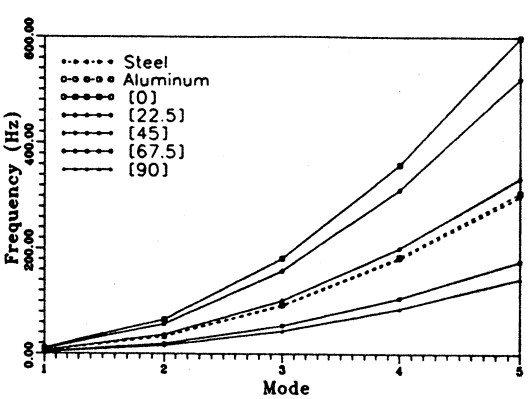

Fig. 10. Frequency variation of fiber angle for carbon/N5280 composite material, with a tubular cross-section.

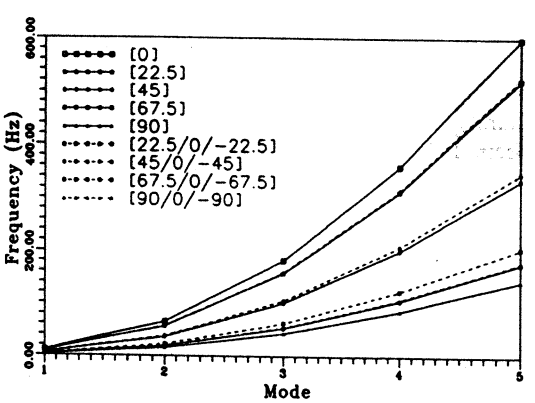

Fig. 11. Frequency of carbon/N5208 composite material, in a different layup, with a tubular cross-section.

is less than that of the steel material. Natural frequencies of carbon/N5280 are less than the steel material when the fiber angle is greater than 50° as shown in Fig. 4. The more 0° layers, the higher natural frequency of the system. The 0° fiber angle in all layers provides the highest natural frequency as shown in Figs 5, 7, 9, 11, 13 and 15. Carbon/N5280 provides the highest natural frequency due to the highest stiffness-to-weight ratio as shown in Figs 16 and 17. The thickness of the layers does not influence the natural frequencies due to the symmetry o the cross-section with respect to neutral axis, a can be seen from eqn (7). The natural frequencies o steel and aluminum beams are the same due to th same stiffness-to-weight ratio of both materials However, the equivalent external load (load/density to the system with aluminum material is greate than that with steel material. For this reason the aluminum material system experiences large deformations.

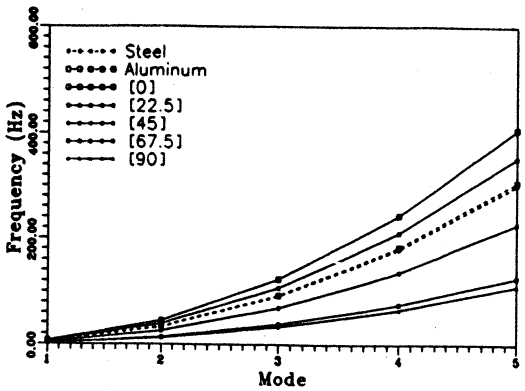

Fig. 12. Frequency variation of fiber angle for Kevlar-49/epoxy composite material, with a tubular cross-section.

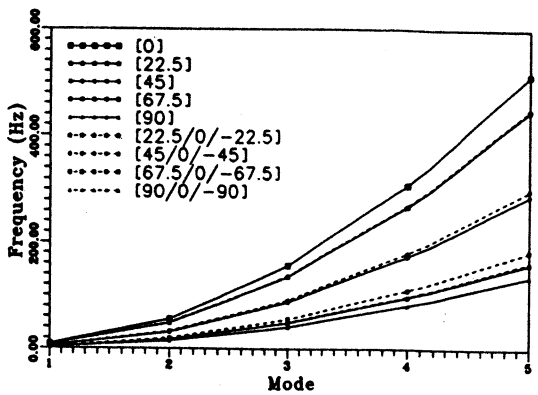

Fig. 15. Frequency, of graphite/epoxy composite material, in a different layup, with a tubular cross-section.

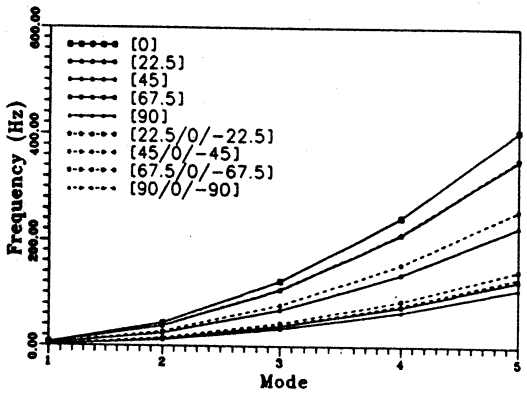

Fig. 13. Frequency of Kevlar-49/epoxy composite material, in a different layup, with a tubular cross-section.

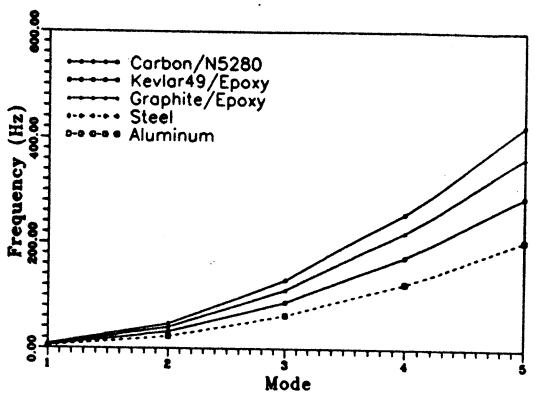

Fig. 16. Natural frequency of different materials with rectangular cross-section.

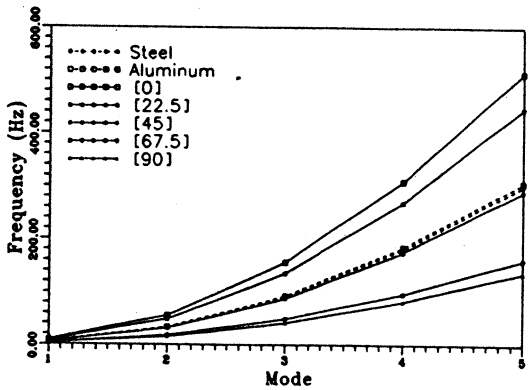

Fig. 14. Frequency variation of fiber angle for graphite/epoxy composite material, with a tubular cross-section.

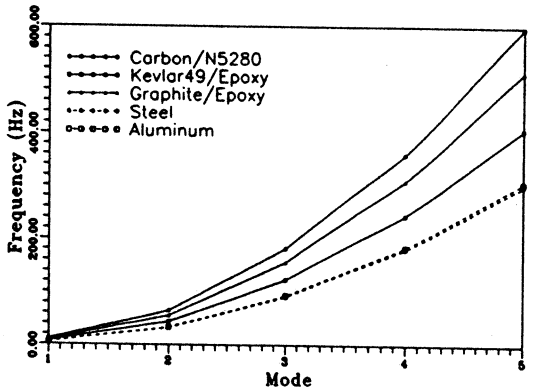

Fig. 17. Natural frequency of different materials with tubular cross-section.

Validation of the present formulation is presented by comparison with the analytical solution for the transverse vibration of the beam structure [28]. An approximation to the governing equation of a rectangular laminated beam in transverse vibration can be derived from the traditional isotropic material problem by substituting EI with bD_{11} [28] (see [29] for an exact formulation)

$$bD_{11}\frac{\partial^4 w}{\partial x^4}+\rho A\frac{\partial^2 w}{\partial t^2}=0. \tag{20}$$

The natural frequency and the mode shape depend on the boundary condition of the beam. The comparison between the analytical and the finite element solution in this paper is given in Table 3 for fixed–free ends. A total of five linear elements was used to model the length of the beam with 0° layup. The material properties and geometrical parameters are given in Tables 1 and 2. The numerical solution validates that the formulation of the mass and the stiffness matrices developed in this paper.

Table 3. Comparison results of analytical method and FEM

	Carbon/N5280		Kevlar-49/epoxy		Graphite/epoxy	
Node	Analytical	Present analysis	Analytical	Present analysis	Analytical	Present analysis
1	7.34638	7.34661	4.98922	4.98931	6.31053	6.31264
2	46.03922	46.06278	31.26706	31.28269	39.54763	39.56743
3	128.91107	129.37574	87.54862	87.86316	110.73446	111.13215
4	250.91829	255.57972	170.40857	173.57235	215.53852	219.53982
5	417.59052	424.19880	283.60230	288.08681	358.70978	364.38143

APPLICATION

In this section, a flexible rotating beam is considered in the application of the matrices developed in this study. Figure 18 shows the configuration in finite element model of a flexible rotating beam system. The finite element method in this type of problem has been well developed and the approach can be referred to in [5].

Based on the small linear deformation, the equations of motion can be expressed in matrix forms as follows:

$$\begin{bmatrix} \mathbf{m}_{\theta\theta} & \mathbf{m}_{\theta f} \\ \mathbf{m}_{f\theta} & \mathbf{m}_{ff} \end{bmatrix} \begin{Bmatrix} \ddot{\theta} \\ \ddot{q}_f \end{Bmatrix} + \begin{bmatrix} 0 & 0 \\ 0 & \mathbf{K}_{ff} \end{bmatrix} \begin{Bmatrix} \theta \\ q_f \end{Bmatrix} = \begin{Bmatrix} \mathbf{F}_{e\theta} \\ \mathbf{F}_{ef} \end{Bmatrix} + \begin{Bmatrix} \mathbf{Q}_{v\theta} \\ \mathbf{Q}_{vf} \end{Bmatrix}, \tag{21}$$

where θ is the rigid body motion generalized coordinate; $\mathbf{q}_f$ are the overall elastic generalized coordinates of the nodes; $\mathbf{m}_{ff}$ and $\mathbf{K}_{ff}$ are the global mass and stiffness matrices; $\mathbf{F}_{e\theta}$ and $\mathbf{F}_{ef}$ are generalized forces; and $\mathbf{Q}_{v\theta}$ and $\mathbf{Q}_{vf}$ are the quadratic velocity vectors resulting from differentiating the kinetic energy with respect to time and with respect to the body coordinates. Equation (21) can be expressed in a concise form

$$[M]\{\ddot{q}\} + [K]\{q\} = \{F_e\} + \{Q_v\}. \tag{22}$$

Due to the coupled effect between rigid body motion and elastic deformation, the equations of motion are nonlinear; the nonlinearity being attributed to the time dependency of the mass matrix. The time-dependent mass matrix contains the generalized elastic coordinates. In linear elastodynamics theory, the coupled effect neglects such that the forward dynamics analysis can be applied to a specific prescribed motion. However, this simplification can cause inaccuracy in simulating the dynamic behavior of the system. In order to maintain the equations of motion with the time variation of the mass matrix and the coupled effect, the inverse dynamic procedure is performed without any simplifications. The beam rotates under a prescribed torque in horizontal plane without any other external load. The prescribed torque is given

$$T(t) = \begin{cases} 4t & \text{(lb-inch)} \quad 0 \leqslant t \leqslant 2 \\ 8 & \text{(lb-inch)} \quad 2 < t \leqslant 4 \\ 8 - 4t & \text{(lb-inch)} \quad 4 < t \leqslant 6. \end{cases} \tag{23}$$

In this numerical simulation, a total of three linear elements were used to model the length of the beam with a 0° layup. A small integration time step must be selected in order to obtain the accurate solution for such type of stiffened system. The predict–corrector Adams–Moulton algorithm is used in this example [30]. However, the carbon/N5280 material cannot converge no matter how small the time step due to the high stiffness-to weight ratio. The material and geometry parameters are given in Tables 1 and 2 for a rectangular cross-section and for a length of 60 in.

Four materials are selected in this simulation: steel, aluminum, Kevlar-49/epoxy, and graphite/epoxy. The major difference relies on the stiffness-to-weight ratio of each material. The responses of angular displacement and acceleration of the isotropic beam in rigid body motion are shown in Figs 19 and 20 respectively. The corresponding responses of the composite beam are shown in Figs 22 and 23. It is observed that, as shown in Fig. 19, the total angular displacement of the steel beam is about one and a half revolutions. On the contrary, the total angular displacement of the graphite beam is about seven revolutions. Lower power consumption is required for the beam with a higher stiffness-to-weight ratio in the same angular displacement occurs. Although the steel and the aluminium have the same stiffness-to-weight ratio, the aluminium material has a higher equivalent external load (load/density) so that the aluminium material experiences larger deflection compared to the steel material. The influence o

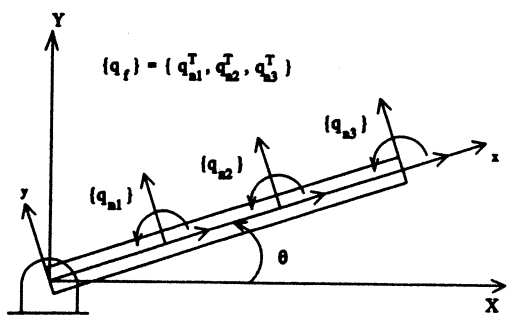

Fig. 18. General finite element configuration of flexible beam.

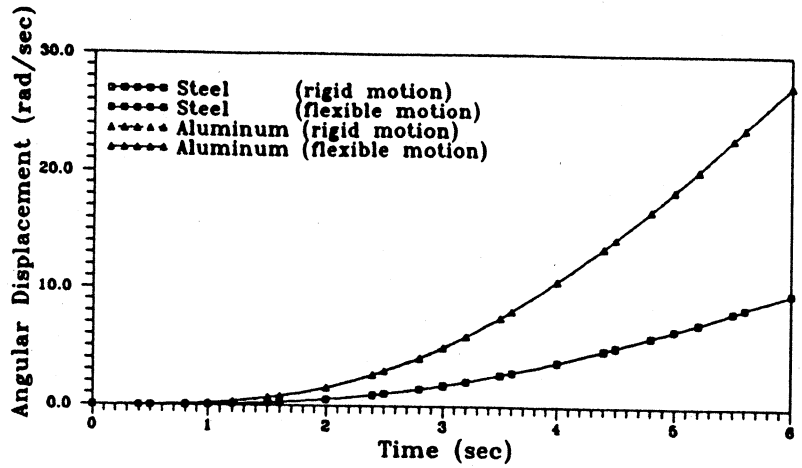

Fig. 19. Angular displacement of the rotating isotropic material beam.

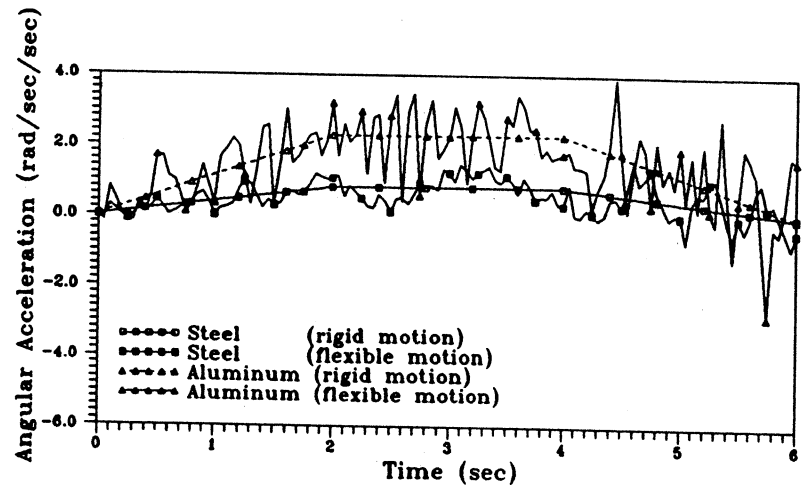

Fig. 20. Angular acceleration of the rotating isotropic material beam.

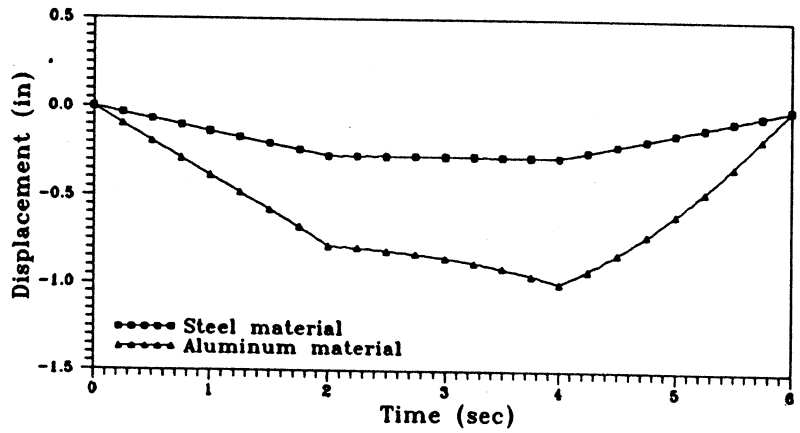

Fig. 21. End point displacement of the rotating isotropic beam.

flexibility on the angular displacement is minimal. The flexibility effect on the angular acceleration is important for all selected materials.

As in Figs 21 and 24 show the transverse deformations are dominated by the angular acceleration. In Fig. 20 the steel beam subjected to a maximum angular acceleration of 0.8 (rad/sec/sec) experiences a maximum deformation of 0.28 in as shown in Fig. 21. However, as shown in Figs 23 and 24, the correspondence of angular acceleration and maximum deformation are 4 (rad/sec/sec) and 0.45 in with graphite/epoxy material. The angular acceleration

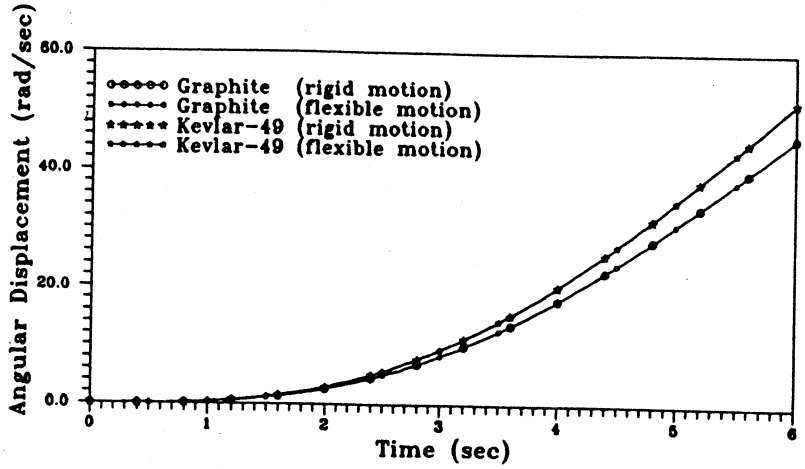

Fig. 22. Angular displacement of the rotating composite material beam.

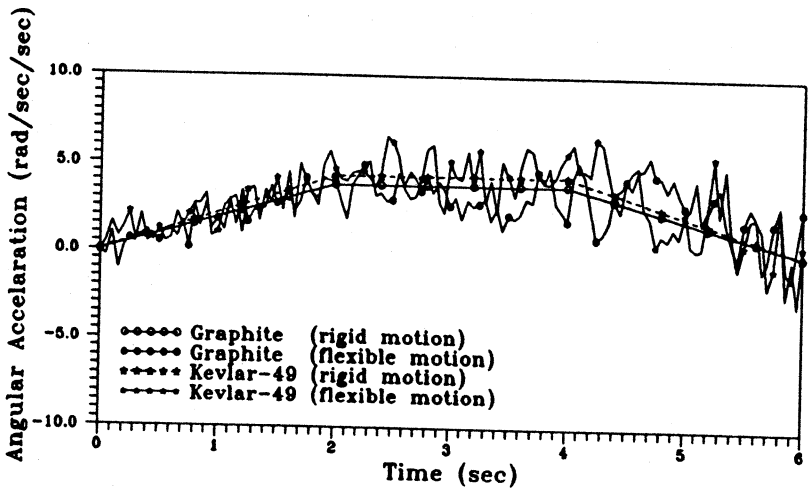

Fig. 23. Angular acceleration of the rotating composite material beam.

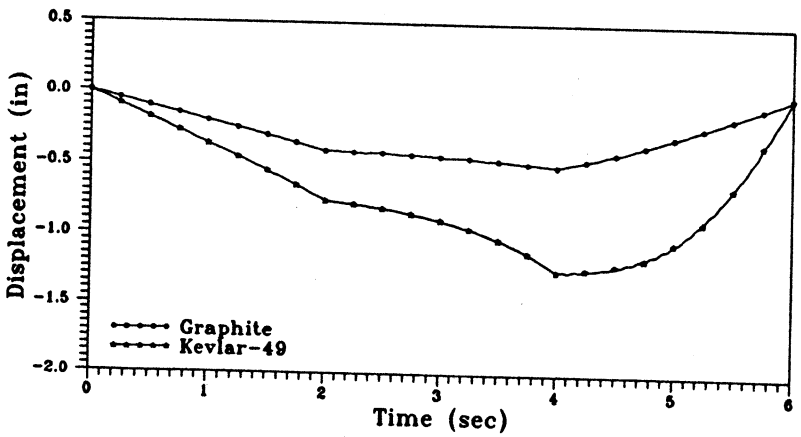

Fig. 24. End point displacement of the rotating composite beam.

with graphite/epoxy material is five times higher than that of steel material but the maximum deformation is about two times greater than that of the steel material. On the other hand, the composite material can be subjected to higher inertial forces. This can be attributed to the high performance of the stiffness-to-weight ratio in composite materials. The maximum deformation in the linear deformation model is about 50% greater than that of geometry nonlinearity deformation for both materials. Therefore, the correct mathematical model is indispensable for more accurate analysis of realistic flexible structure systems.

CONCLUSIONS

The free vibration natural frequency analysis of a helically wound tubular and laminated beam composite material has been investigated in this paper. Based on the shell lamination theory and small deformation assumption, the mass and stiffness finite element matrices of a helically wound tubular beam have been derived. Each element has three degrees of freedom: axial, transverse, and rotation. The mass and the stiffness matrices derived from the helically wound element are also reduced to the orthotropic fiber-reinforced symmetrical laminated composite beam. These matrices can be used for the dynamic analysis of multibody flexible systems with composite material links. The natural frequency of the beam element depends on the layup and the stiffness-to-weight ratio.

A flexible rotating beam is investigated in this application. The dynamic model of the flexible rotating beam includes the coupled effect between the rigid body motion and the flexible motion. The equations of motion of the flexible rotating beam are nonlinear with time-dependent coefficients and are expressed in terms of the elastic generalized coordinates and the large angular displacement of the beam. The inverse dynamic simulation is performed by a prescribed driving torque in the numerical simulation. The responses of the transverse deformation and the influence of the flexibility on the rigid body motion are evaluated and discussed. For the composite material it is shown that it strongly possesses lower power consumption and the passive control in damping the vibration of the structure.

In future work, shear deformation and geometrical nonlinearity will be considered for more accurate modeling of realistic system such as robotic manipulators, rotating blades and mechanisms, built with composite materials.

REFERENCES

1. A. G. Erdman and G. N. Sandor, Kineto-elastodynamics—a review of the state-of-the-art and trends. *Mechanism and Machine Theory* **7**, 3–17 (1972).
2. J. O. Song and E. J. Haug, Dynamic analysis of planar flexible mechanism. *Comput. Meth. Appl. Mech. Engng* **24**, 359–381 (1980).
3. D. Trucic and A. Midha, Generalized equations of motion for the dynamic analysis of elastic mechanism systems. *J. Dynamic Systems, Measurements and Controls* **106**, 243–248 (1984).
4. O. P. Agrawel and A. A. Shabana, Dynamic analysis of multi-body systems using components modes. *Comput. Struct.* **21**, 1303–1312 (1985).
5. A. A. Shabana, *Dynamics of Multibody Systems*. John Wiley (1989).
6. V. H. Mucino, C. I. Chen and N. T. Sivaneri, A continuous based Hamilton–Lagrange approach to the elastodynamics of flexible mechanisms. *Proceedings of Oklahoma State University's 10th Applied Mechanisms Conference*, New Orleans, LA (1987).
7. M. Badlani and A. Midha, Effect of internal material damping of the dynamics of a slider–crank mechanism. *J. Mechanisms, Transmissions, and Automation in Design* **105**, 452–459 (1983).
8. P. K. C. Wang and Jin-Duo Wei, Variations in a moving flexible robot arm. *J. Sound Vibr.* **116**, 149–160 (1987).
9. V. Masurekar and K. N. Gupta, Stability analysis of four bar mechanism. Part I—with the assumption that damping is absent. *Mechanism and Machine Theory* **23**, 367–375 (1988).
10. Z. E. Boutaghou, K. K. Tamma and A. G. Erdman, Continuous/discrete modelling and analysis of elastic planar multi-body systems. *Comput. Struct.* **38**, 605–613 (1991).
11. E. R. Christensen and S. W. Lee, Nonlinear finite element modeling of the dynamics of unrestrained flexible structures. *Comput. Struct.* **23**, 819–829 (1986).
12. F. Van Der Weeën, A finite element approach to three-dimensional kineto-elastodynamics. *Mechanism and Machinery Theory* **23**, 491–500 (1988).
13. W. L. Cleghorn and K. C. Chao, Kineto-elastodynamic modelling of mechanisms employing linearly tapered beam finite elements. *Mechanism and Machine Theory* **23**, 333–342 (1988).
14. Zhijia Yang and J. P. Sadler, Large-displacement finite element analysis of flexible linkages. *J. Mech. Design* **112**, 175–182 (1990).
15. P. Kalra and A. M. Sharan, Accurate modeling of flexible manipulators using finite element analysis. *Mechanism and Machine Theory* **26**, 299–313 (1991).
16. A. A. Shabaha and R. A. Wehage, Variable degree-of-freedom component mode analysis of inertia variant flexible mechanical systems. *J. Mechanisms, Transmissions, and Automation in Design* **105**, 391–378 (1983).
17. A. A. Shabaha and R. A. Wehage, Spatial transient analysis of inertia-variant flexible mechanical systems. *J. Mechanisms, Transmissions, and Automation in Design* **106**, 172–106 (1984).
18. B. S. Thompson, D. Zuccaro, D. Gamache and M. V. Gandhi, An experimental and analytical study of a four bar mechanism. *Mechanism and Machine Theory* **18**, 165–171 (1983).
19. C. K. Sung and B. S. Thompson, Material selection: an important parameter in design of high-speed linkages. *Mechanism and Machine Theory* **19**, 389–396 (1984).
20. B. S. Thompson and C. K. Sung, A variational formulation for the dynamic viscoelastic finite element analysis of robotic manipulators constructed from composite materials. *J. Mechanisms, Transmissions, and Automation in Design* **106**, 183–190 (1984).
21. B. S. Thompson and C. K. Sung, An analytical and experimental investigation of high-speed mechanisms fabricated with composite laminates. *J. Sound Vibr* **111**, 399–428 (1986).
22. A. A. Shabana, Effect of using composites on the dynamic response of multi-body systems. *J. Sound Vibr.* **108**, 487–502 (1986).
23. J. G. D'Acquisto, Helically wound composites for performance enhancement of flexible linkages. M.S.M.E. Thesis, College of Engineering, West Virginia University (1988).
24. K. Krishnamurthy, K. Chandrashekhara and S. Roy, A study of single-link robots fabricated from orthotropic composite materials. *Comput. Struct.* **36**, 139–146 1990.
25. A. T. Chen and T. Y. Yang, Static and dynamic formulation of a symmetrically laminated beam finite element for a microcomputer. *J. Compos. Mater.* **19**, 459–475 (1985).
26. R. M. Jones, *Mechanics of Composite Materials*. McGraw-Hill, New York (1975).
27. W. Flugge, *Stresses in Shells*. Springer, Berlin (1962).
28. J. R. Vinson and R. L. Sierakowski, *The Behavior of Structures Composed of Composite Materials*. Martinus Nijhoff, Dordrecht (1987).
29. E. J. Barbero, R. Lopez-Anido and J. F. Davalos, On the mechanics of thin-walled laminated composite beams. *J. Compos. Mater.* **27**, 806–829 (1993).
30. Conte and de Boor, *Elementary Numerical Analysis*, 3rd Edn, McGraw-Hill (1980).

APPENDIX

$$[M] = \rho_m A l \begin{bmatrix} \frac{1}{3} & 0 & 0 & \frac{1}{6} & 0 & 0 \\ 0 & \frac{13}{35} & \frac{11l}{210} & 0 & \frac{9}{70} & -\frac{13l}{420} \\ 0 & \frac{11l}{210} & \frac{l^2}{105} & 0 & \frac{13l}{520} & -\frac{l^2}{140} \\ \frac{1}{6} & 0 & 0 & \frac{1}{3} & 0 & 0 \\ 0 & \frac{9}{70} & \frac{13l}{420} & 0 & \frac{13}{35} & -\frac{11l}{210} \\ 0 & -\frac{13l}{420} & -\frac{l^2}{140} & 0 & -\frac{11l}{210} & \frac{l^2}{105} \end{bmatrix}$$

$$[K] = 2\pi a \begin{bmatrix} \frac{\beta_1}{l} & 0 & -\frac{\beta^2}{l} & -\frac{\beta_1}{l} & 0 & \frac{\beta_2}{l} \\ 0 & \frac{12\beta_3}{l^3} & \frac{6\beta_3}{l^2} & 0 & -\frac{12\beta_3}{l^3} & \frac{6\beta_3}{l^2} \\ -\frac{\beta_2}{l} & \frac{6\beta_3}{l^2} & \frac{4\beta_3}{l} & \frac{\beta_2}{l} & -\frac{6\beta_3}{l^2} & \frac{2\beta_3}{l} \\ -\frac{\beta_1}{l} & 0 & \frac{\beta_2}{l} & \frac{\beta_1}{l} & 0 & -\frac{\beta_2}{l} \\ 0 & -\frac{12\beta_3}{l^3} & -\frac{6\beta_3}{l^2} & 0 & \frac{12\beta_3}{l^3} & -\frac{6\beta_3}{l^2} \\ \frac{\beta_2}{l} & \frac{6\beta_3}{l^2} & \frac{2\beta_3}{l} & -\frac{\beta_2}{l} & -\frac{6\beta_3}{l^2} & \frac{4\beta_3}{l} \end{bmatrix},$$

where

$$\beta_1 = A_{11} + \frac{B_{11}}{a}$$

$$\beta_2 = B_{11} + \frac{D_{11}}{a}$$

$$\beta_3 = D_{11}.$$